

# Chapter 2

## Photovoltaic and Pyroelectric Solitons



### 2.1 The Photovoltaic Effect

The conventional photovoltaic effect is a phenomenon which describes the generation of a voltage or electric current in a photovoltaic cell when sunlight is incident upon it. The cells within a solar panel convert sunlight to electrical energy. The solar cells are made of two joined *p*-type and *n*-type semiconductors which result in a *p*-*n* junction. A space charge field is formed at the junction as electrons diffuse to the *p*-side and holes diffuse to the *n*-side. This field causes a potential difference which can be harnessed as electrical energy.

The photovoltaic effect in which we are interested is different from the above described *p*-*n* junction photovoltaic effect described in solar cells. The bulk photovoltaic effect is known to occur in semiconductors and insulators. The bulk photovoltaic effect is also known to as “anomalous”. That is so because the typical photovoltage produced by incident light is much greater than the band gap of the semiconductor. In certain crystals, the photovoltage may be of the order of  $\sim 10^3$  V.

The main phenomenon behind the bulk photovoltaic effect is that various electron related processes occur with different rates in different directions. Photo-excitation, scattering, and relaxation have a different probability of occurring in different directions with respect to the motion of the electron. This results in generation of a large photovoltage [1, 2].

Another mechanism involves development of parallel stripes ferroelectric domains in certain materials. Each domain acts like a photovoltaic and the domain wall behaves like a contact connecting the adjacent photovoltaics. The domains add in series, and hence the overall open-circuit voltage is quite large.

In Fig. 2.1, a simple system is illustrated through which we can understand the bulk photovoltaic effect. Consider two electronic levels separated by an energy gap of say, 3 eV in a unit cell. The blue and pink arrows show radiative and non radiative transitions respectively. An electron can move from A to B by absorbing a photon. Conversely, it may move from B to A by emitting a photon. The purple arrows indicate non radiative transitions. Here, it is implied that an electron can move from

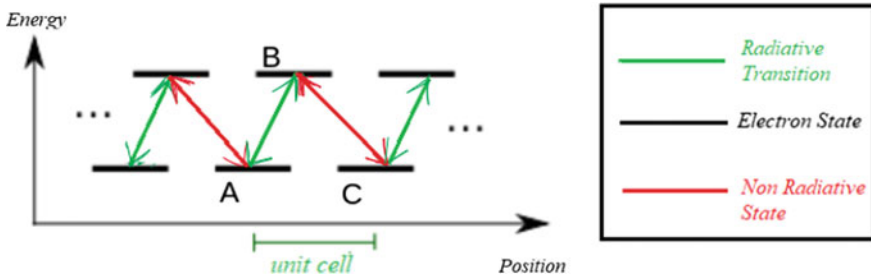


**Fig. 2.1** The photovoltaic effect illustrated

B to C via lattice vibrations or emitting phonons, or vice versa by absorption of phonons.

If a light beam is incident upon a photovoltaic crystal, considering the above scenario, an electron can go from A to B to C by absorbing photons. But, the electron does not move in the opposite direction, i.e., from C to A through B, since the shift from C to B proceeds if a large thermal variation is present which in turn is improbable. Hence, we see a net rightward photocurrent.

There are many interesting features of the bulk photovoltaic effect distinguishing it from the conventional photovoltaic effect. Within the region of power generation in the characteristic I-V curve, electrons and holes are moved towards higher and lower Fermi levels respectively. We expect the opposite based on the drift diffusion equation. For example, power generation in a silicon solar cell is possible due to splitting of the quasi-Fermi levels which implies the fact that the motion of electrons is towards the decreasing quasi-Fermi level and the motion of holes is towards the increasing quasi-Fermi level as per the drift diffusion equation. In contrast, power is generated in a bulk photovoltaic without any splitting of quasi-Fermi levels.

The drift diffusion effect predicts that freely moving electrons will lessen the photocurrent and consequently diminish the photovoltaic effect. So, appreciable open-circuit voltages are observed only in crystals that exhibit very low dark conductivity.

The net motion of electrons due to the bulk photovoltaic effect is in the opposite direction to that expected due to the drift-diffusion equation. Hence, the quantum efficiency lessens considerably even for a thick device. Large amount of photons (of the order of  $10^6$ ) may be needed to transport an electron between the two electrodes. An increase in thickness results in voltage going up and a decrease in current. Also, the current may have different directions depending on the light polarization. Such effects are unheard of in silicon or any other ordinary solar cell.

## 2.2 Screening Photovoltaic Solitons

### 2.2.1 Theoretical Foundation

Until now, we have considered an externally biased non photovoltaic photorefractive crystal for studying steady state optical spatial solitons. However, if we take a photorefractive crystal also having a finite photovoltaic coefficient, the question arises as to whether it can support optical spatial solitons in the presence of an external bias? In [3], the authors have studied this in detail and we shall study these screening photovoltaic solitons in this section. Taking the electric field envelope as  $\vec{E} = \hat{x}\phi(x, z)\exp(ikz)$ , the paraxial equation of diffraction is [4],

$$i \frac{\partial \phi}{\partial z} + \frac{1}{2k} \frac{\partial^2 \phi}{\partial x^2} - \frac{k_0 n_e^3 r_{eff} E_{sc}}{2} \phi = 0 \quad (2.1)$$

The induced space charge field can be derived from the set of rate equations, continuity equations and Gauss law in one dimension for steady state [5],

$$\gamma_R n N_D^+ = s_i (I + I_d) (N_D - N_D^+) \quad (2.2)$$

$$\frac{\partial E_{sc}}{\partial x} = \frac{e}{\epsilon_0 \epsilon} (N_D^+ - N_A - n) \quad (2.3)$$

$$J = e \mu n E_{sc} + k_B T \mu \frac{\partial n}{\partial x} + k_p s_i (N_D - N_D^+) I \quad (2.4)$$

$$\frac{\partial J}{\partial x} = 0 \quad (2.5)$$

where the symbols have their usual meanings. There is one change in these equations if we compare them with those used in previous chapters. We have now considered  $k_p$  to be the photovoltaic constant which contributes the photovoltaic current term. As usual, any  $z$  spatial dependence has been ignored assuming a much more rapid variation in  $x$ . Now, in typical photovoltaic-photorefractive media,  $N_D^+ \gg n$ ,  $N_D \gg n$ , and  $N_A \gg n$ . Hence, (2.2) and (2.3) give,

$$N_D^+ = N_A \left( 1 + \frac{\epsilon_0 \epsilon_r}{e N_A} \frac{\partial E_{sc}}{\partial x} \right) \quad (2.6)$$

$$n = \frac{s_i (N_D - N_A)}{\gamma_R N_A} (I + I_d) \left( 1 + \frac{\epsilon_0 \epsilon_r}{e N_A} \frac{\partial E_{sc}}{\partial x} \right)^{-1} \quad (2.7)$$

If the intensity of the light beam varies relatively slowly with respect to  $x$ , the term  $\frac{\epsilon_0 \epsilon_r}{e N_A} \frac{\partial E_{sc}}{\partial x}$  can be ignored, as it is of the order of much less than unity. So, from

(2.6) and (2.7) it can be inferred that,

$$N_D^+ = N_A \quad (2.8)$$

$$n = \frac{s_i(N_D - N_A)}{\gamma_R N_A} (I + I_d) \quad (2.9)$$

In regions of constant illumination, we know,  $I(x \rightarrow \pm\infty, z) = I_\infty$ ,  $E_{sc}(x \rightarrow \pm\infty, z) = E_0$  where  $E_0$  is the external bias field. From (2.7), electron density at  $x \rightarrow \pm\infty$ , i.e.,  $n_\infty$  can be obtained as,

$$n_\infty = \frac{s_i(N_D - N_A)}{\gamma_R N_A} (I_\infty + I_d) \quad (2.10)$$

From (2.4), we know that,

$$J_\infty = J(x \rightarrow \pm\infty, z) = e\mu n_\infty E_0 + k_p s_i (N_D - N_A) I_\infty \quad (2.11)$$

Substituting (2.10) into (2.11),

$$J_\infty = e\mu n_\infty \left( E_0 + E_p \frac{I_\infty}{I_\infty + I_d} \right) \quad (2.12)$$

where,  $E_p = k_p \gamma_R N_A / (e\mu)$ .

Again, from (2.2) and (2.4), we get,

$$J = e\mu n \left( E_{sc} + \frac{k_B T}{e} \frac{\partial \ln n}{\partial x} + E_p \frac{I}{I + I_d} \right) \quad (2.13)$$

From (2.5), we can infer that the current is constant everywhere, so, from (2.12) and (2.13),

$$n_\infty \left( E_0 + E_p \frac{I_\infty}{I_\infty + I_d} \right) = n \left( E_{sc} + \frac{k_B T}{e} \frac{\partial \ln n}{\partial x} + E_p \frac{I}{I + I_d} \right) \quad (2.14)$$

Finally, we can obtain the space charge field from (2.14) as,

$$E_{sc} = E_0 \frac{I_\infty + I_d}{I + I_d} + E_p \frac{I_\infty - I}{I + I_d} - \frac{k_B T}{e} \frac{1}{I + I_d} \frac{\partial I}{\partial x} \quad (2.15)$$

The final dynamical evolution equation can now be setup by substituting (2.15) into (2.1),

$$i \frac{\partial U}{\partial \xi} + \frac{1}{2} \frac{\partial^2 U}{\partial s^2} - \beta(\rho + 1) \frac{1}{1 + |U|^2} U - \alpha \frac{(\rho - |U|^2)}{1 + |U|^2} U + \gamma \frac{(|U|^2)_s}{1 + |U|^2} U = 0 \quad (2.16)$$

where we use the dimensionless co-ordinates,  $\xi = z/(kx_0^2)$ ,  $s = x/x_0$ ,  $\phi = (2\eta_0 I_d/n_e)^{1/2} U$  with  $x_0$  to be an arbitrary spatial width and the intensity scaled with the dark irradiance  $I_d$ ,  $\rho = I_\infty/I_d$ ,  $\beta = (k_0 x_0)^2 (n_e^4 r_{eff}/2) E_0$ ,  $\alpha = (k_0 x_0)^2 (n_e^4 r_{eff}/2) E_p$ ,  $\gamma = (k_0^2 x_0 n_e^4 r_{eff}) k_B T / (2e)$ .

### 2.2.2 Spatial Soliton States

Once the dynamical evolution (2.16) has been obtained, it is a simple matter now to solve this get soliton states. As earlier, we proceed to solve the PDE by numerical techniques. Considering first the bright solitons,  $\rho = 0$ , and hence, (2.16) becomes,

$$i \frac{\partial U}{\partial \xi} + \frac{1}{2} \frac{\partial^2 U}{\partial s^2} - \beta \frac{1}{1 + |U|^2} U - \alpha \frac{(|U|^2)}{1 + |U|^2} U + \gamma \frac{(|U|^2)_s}{1 + |U|^2} U = 0 \quad (2.17)$$

Again, neglecting the effect of diffusion which is plausible if we consider a large value of the photovoltaic and bias field,

$$i \frac{\partial U}{\partial \xi} + \frac{1}{2} \frac{\partial^2 U}{\partial s^2} - \beta \frac{1}{1 + |U|^2} U - \alpha \frac{(|U|^2)}{1 + |U|^2} U = 0 \quad (2.18)$$

Substituting the bright soliton solution ansatz  $U = r^{1/2} y(s) \exp(iv\xi)$ , where  $r = I(0)/I_d$  and  $0 \leq y(s) \leq 1$  along with the requisite boundary conditions of bright solitons as discussed before in (2.18), we get,

$$\ddot{y} - 2vy - 2\beta \frac{y}{1 + ry^2} + 2\alpha \frac{ry^3}{1 + ry^2} = 0 \quad (2.19)$$

where  $\ddot{y} = \frac{d^2 y}{ds^2}$ .

Integrating (2.19) once and applying the boundary conditions,

$$v = -\frac{\beta + \alpha}{r} \ln(1 + r) + \alpha \quad (2.20)$$

$$(\dot{y})^2 = 2 \frac{(\beta + \alpha)}{r} [-y^2 \ln(1 + r) + \ln(1 + ry^2)] \quad (2.21)$$

The bright field profile can now found by numerical integration as follows,

$$[2(\beta + \alpha)]^{1/2}s = \pm \int_y^1 \frac{r^{1/2}d\hat{y}}{[\ln(1 + r\hat{y}^2) - \hat{y}^2\ln(1 + r)]^{1/2}} \quad (2.22)$$

In (2.21), we can clearly see that the quantity in square brackets is positive since  $y(s)$  is bounded between 0 and 1, and since the LHS is also necessarily positive, we get the condition  $\beta + \alpha > 0$  for existence of screening photovoltaic bright solitons.

For the dark screening photovoltaic solitons, substituting the appropriate ansatz  $U = \rho^{1/2}y(s)\exp(iv\xi)$  along with the dark soliton boundary conditions as stated before,  $y(0) = 0$ ,  $\dot{y}(0) = 0$ ,  $y(s \rightarrow \pm\infty) = 1$  in (2.16) and neglecting the diffusion effect,

$$\ddot{y} - 2vy - 2\beta(\rho + 1)\frac{y}{1 + \rho y^2} - 2\alpha\rho\frac{\rho y^3}{1 + \rho y^2} = 0 \quad (2.23)$$

Using the boundary conditions, one can readily deduce that,

$$v = -\beta \quad (2.24)$$

$$(\dot{y})^2 = 2(\beta + \alpha)\left[(y^2 - 1) - \frac{\rho + 1}{\rho}\ln\left(\frac{1 + \rho y^2}{1 + \rho}\right)\right] \quad (2.25)$$

The soliton field profile can be obtained by numerical integration of (2.25) as follows,

$$[2(\beta + \alpha)]^{1/2}s = \pm \int_y^0 \frac{d\hat{y}}{\left[(\hat{y}^2 - 1) - \frac{\rho + 1}{\rho}\ln\left(\frac{1 + \rho\hat{y}^2}{1 + \rho}\right)\right]^{1/2}} \quad (2.26)$$

In (2.25), the quantity in square brackets is positive since  $y(s)$  is bounded below one, and hence, we can see clearly that  $\beta + \alpha < 0$  should be satisfied for the RHS to remain positive.

What we can infer from this discussion is that bright or dark solitons can be obtained in photovoltaic photorefractive crystals for suitable conditions. For instance, in Lithium Niobate crystals, where  $\alpha < 0$ , if the external applied bias field is such that  $|\beta| < |\alpha|$ , then dark solitons can be observed irrespective of the polarity of the external electric field. Again, there are some photovoltaic materials where the photovoltaic constant changes sign under polarization rotation and hence  $\alpha$  will be positive or negative depending on the polarization of light. In case  $\alpha > 0$ , the polarity of the external electric field must be reversed to observe dark solitons. Using the values of the Lithium Niobate Crystals as shown in Table 2.1, the normalized intensities of the dark solitons using (2.26) are plotted in Fig. 2.2.

For the grey solitons, we shall employ the grey soliton ansatz,  $U(s, \xi) = \rho^{1/2}y(s)\exp\left[i\left(v\xi + \int \frac{Qds}{y^2(s)}\right)\right]$  along with the grey soliton boundary conditions,

**Table 2.1** Typical parameters used for lithium niobate crystal in the calculation [3]

Parameter	Value	Parameter	Value
$\lambda_0$	0.5 $\mu\text{m}$	$\alpha$	-355.13
$x_0$	40 $\mu\text{m}$	$E_0$	(a) $2 \times 10^6 \text{ Vm}^{-1}$ (b) $-2 \times 10^6 \text{ Vm}^{-1}$
$n_e$	2.2	$\beta$	(a) 177.57, (b) -177.57 (respectively to $E_0$ )
$r_{33}$	$30 \times 10^{-12} \text{ mV}^{-1}$	$\rho$	10
$E_p$	$4 \times 10^6 \text{ Vm}^{-1}$		

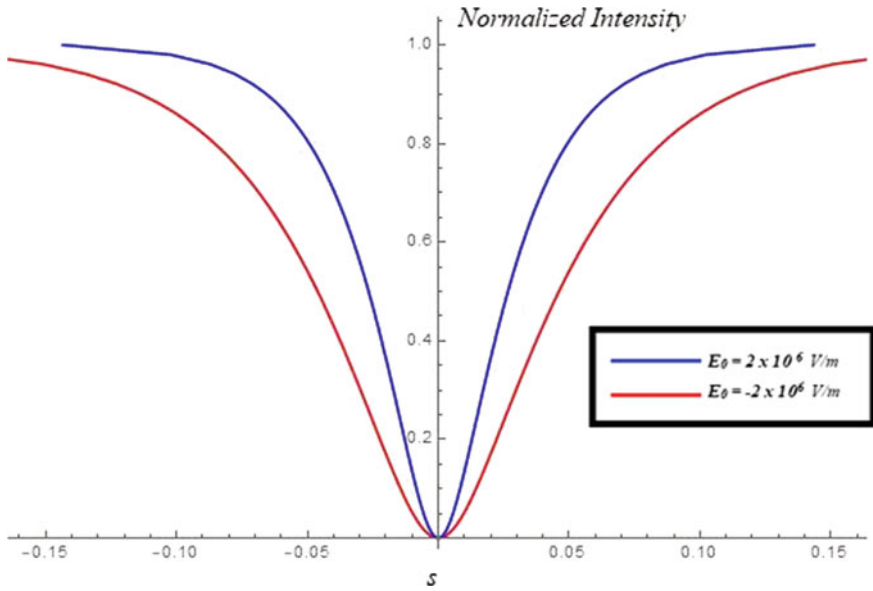


**Fig. 2.2** Normalized spatial profiles for the dark screening photovoltaic soliton [3]

$y^2(s=0) = m$  ( $0 < m < 1$ ),  $y(s \rightarrow \pm\infty) = 1$ ,  $\dot{y}(0) = 0$ . Hence, (2.16) becomes,

$$\ddot{y} - 2vy - \frac{Q^2}{y^3} - 2\beta(1 + \rho) \frac{y}{1 + \rho y^2} - 2\alpha\rho \frac{\rho(1 - y^2)y}{1 + \rho y^2} = 0 \quad (2.27)$$

or,

$$\ddot{y} - 2(v - \alpha)y - \frac{Q^2}{y^3} - 2(\alpha + \beta)(1 + \rho) \frac{y}{1 + \rho y^2} = 0 \quad (2.28)$$

Applying the boundary conditions of the grey solitons at infinity, we have,

$$Q^2 = -2(v + \beta) \quad (2.29)$$

(2.28) yields after an integration,

$$(\dot{y})^2 = 2(v - \alpha)(y^2 - 1) + 2(v + \beta)\left(\frac{1 - y^2}{y^2}\right) + \frac{2(\alpha + \beta)(1 + \rho)}{\rho} \ln\left(\frac{1 + \rho y^2}{1 + \rho}\right) \quad (2.30)$$

Applying the boundary conditions of grey solitons at zero in (2.30), we get,

$$v = \frac{1}{(m - 1)^2} \left[ m(m - 1)\alpha + (m - 1)\beta - \frac{m(\alpha + \beta)(1 + \rho)}{\rho} \ln\left(\frac{1 + \rho m}{1 + \rho}\right) \right] \quad (2.31)$$

From (2.29) and (2.31),

$$(\alpha + \beta) \left[ m(m - 1) - \frac{m(1 + \rho)}{\rho} \times \ln\left(\frac{1 + \rho m}{1 + \rho}\right) \right] < 0 \quad (2.32)$$

Expanding  $\ln\left(\frac{1 + \rho m}{1 + \rho}\right) = \ln\left(\frac{1 + (m-1)\rho}{1 + \rho}\right)$  in series, we can see that the quantity inside the square bracket in (2.32) is positive. That in turn implies the condition for existence of grey solitons in photorefractive photovoltaic media reduces to,  $(\alpha + \beta) < 0$ . Additionally, the values of  $(\alpha, \beta, \rho, m)$  must be chosen judiciously so as to always have  $\dot{y}^2 > 0$  and  $Q^2 > 0$ . Integrating (2.32) once again gives the spatial profile,

$$[-2(\alpha + \beta)]^{1/2} s = \pm \int_{\sqrt{m}}^y (1 - m) \left[ \frac{m(1 + \rho)}{\rho} \times \ln\left(\frac{1 + \rho m}{1 + \rho}\right) \left(\tilde{y}^2 + \frac{1}{\tilde{y}^2} - 2\right) + (1 - m)(\tilde{y}^2 - 1) + \right]^{-1/2} d\tilde{y} \quad (2.33)$$

Using (2.33), the normalized spatial profile of the grey soliton is plotted in Fig. 2.3 using typical parameters of the lithium niobate crystal as shown in Table 2.2. Also, unlike the bright and dark screening photovoltaic solitons, the phase is not constant across  $s$ . This is evident from the grey soliton ansatz and using (2.29) and (2.31). Figure 2.4 shows the phase profile across the grey soliton.

The screening photovoltaic solitons have a different existential theoretical foundation as compared to screening solitons. There is an inherent interplay of the photovoltaic field with the external bias field. It is interesting to note a few special cases here. If  $\alpha = 0$ , i.e., we take a non-photovoltaic crystal in (2.16), we retrieve the bright, dark and grey screening solitons formulation. While if we set  $\beta = 0$ , i.e.,



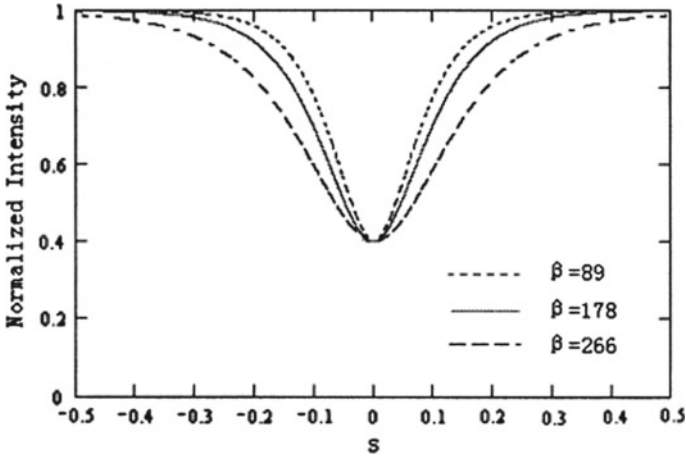
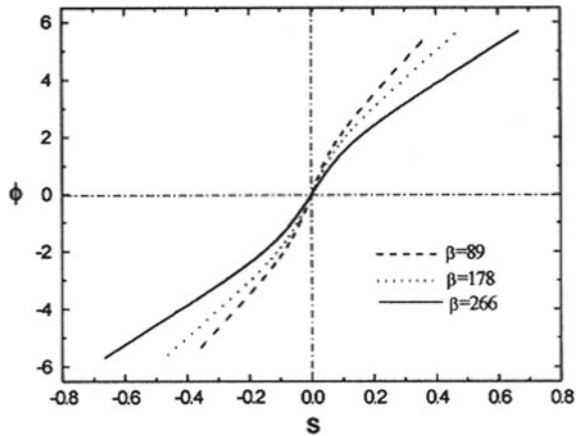


**Fig. 2.3** Normalized spatial profiles for the grey screening photovoltaic soliton (reprinted from Optics Communications, 181, Chunfeng Hou, Yan Li, Xiaofu Zhang, Baohong Yuan, Xiudong Sun, Grey screening-photovoltaic spatial soliton in biased photovoltaic photorefractive crystals., 141–144, Copyright 2000, with permission from Elsevier)

**Table 2.2** Typical parameters used for lithium niobate crystal in the calculation [3]

Parameter	Value	Parameter	Value
$\lambda_0$	0.5 $\mu\text{m}$	$\alpha$	-355
$x_0$	40 $\mu\text{m}$	$E_0$	(a) $1 \times 10^6 \text{ Vm}^{-1}$ (b) $2 \times 10^6 \text{ Vm}^{-1}$ (c) $3 \times 10^6 \text{ Vm}^{-1}$
$n_e$	2.2	$\beta$	(a) 89, (b) 178, (c) 266 (relative to $E_0$ )
$r_{33}$	$30 \times 10^{-12} \text{ mV}^{-1}$	$m$	0.4
$E_p$	$4 \times 10^6 \text{ Vm}^{-1}$	$\rho$	5

**Fig. 2.4** Phase profiles for the grey screening photovoltaic soliton (reprinted from Optics Communications, 181, Chunfeng Hou, Yan Li, Xiaofu Zhang, Baohong Yuan, Xiudong Sun, Grey screening-photovoltaic spatial soliton in biased photovoltaic photorefractive crystals, 141–144, Copyright 2000, with permission from Elsevier)



we switch off the external bias, we obtain the expressions for bright, dark and grey photovoltaic solitons in closed circuit realization ( $J \neq 0$  within the crystal) under suitable values of  $\alpha$ . For bright photovoltaic solitons, we need  $\alpha = r(J + 1)/2$  while for dark solitons we need  $\alpha = -(J + 1)/[2(\rho + 1)]$ .

### 2.2.3 Further Reading

The reader is referred to [6, 7] where the authors have detailed the photovoltaic solitons. The general formulation presented here branches out to systems of photorefractive crystal which is open circuited or closed circuited and without the external bias field.

## 2.3 The Pyroelectric Effect

Pyroelectricity is a phenomenon in which a transient voltage is induced in a material when it is heated or cooled. The reason behind this is that when temperature changes momentarily, atoms move around within the crystal lattice and their positions are modified slightly resulting in a change of net polarization. The net polarization change results in a voltage appearing across the crystal. This induced voltage known is known as the pyroelectric voltage and is transient. It will gradually vanish due to leakage current if the temperature remains constant afterward. The leakage current can be present due to a number of causes like movement of electrons through the crystal, movement of ions through the air, or leakage current through a voltmeter attached across the crystal. Contrasting temperature changes induce opposite charges. If heating induces a positive charge on one face, cooling will induce a negative charge at the same face. Quantitatively, pyroelectricity can be said to be the change in net polarization proportional to a change in temperature. The pyroelectric coefficient is defined as,

$$p_i = \frac{\partial P}{\partial T} \quad (2.34)$$

The total pyroelectric coefficient depends upon the primary as well the secondary pyroelectric effect. At constant stress, the piezoelectric contribution from thermal expansion must be added to the pyroelectric coefficients at constant strain to obtain the total pyroelectric coefficient.

All crystal structures can be classified to belong to a set of thirty-two crystal classes, also known as point groups. Twenty-one of these thirty two are non-centrosymmetric. Again, twenty of these twenty one display direct piezoelectricity. In turn, ten of these twenty piezoelectric classes can be expressed to possess a spontaneous polarization, and hence are known as polar classes. Notable is the fact that

these also contain a dipole in their unit cell in addition to exhibiting pyroelectricity. Such a material is also ferroelectric if an applied electric field reverses the dipole. In summary, out of the 32 crystal classes, 10 are polar. Since all polar crystals are pyroelectric, so these crystal classes are also known as pyroelectric classes.

## 2.4 Pyroelectric Solitons (the “Pyroliton”)

Pyroelectric solitons, or pyrolitons have been subject of intense research in recent times [8–10]. The transient pyroelectric field alone can cause a stable self trapping as we will see in this section. Combing the transient pyroelectric field with the photovoltaic field or the external electric field can yield interesting effects on the self trapping. There are two conditions which need to be satisfied for the formation of such pyroelectric solitons, firstly that the transient pyroelectric field magnitude is relatively large and secondly, that the the pyroelectric field’s relaxation time be greater than the soliton formation time. Assuming the homogeneous heating of a crystal, the pyroelectric field can be expressed as,

$$E_{py} = \frac{1}{\epsilon_0 \epsilon_r} \frac{\partial P}{\partial T} \Delta T \quad (2.35)$$

$\Delta T$  is the temperature change. The relaxation time for the pyroelectric field can be given by,

$$\tau = \frac{\epsilon_0 \epsilon_r}{\sigma_d} \Delta T \quad (2.36)$$

where  $\sigma_d$  is the dark conductivity of the crystal. Taking typical parameters of the  $\text{LiNbO}_3$  crystal ( $\epsilon_r = 28$ ,  $\sigma_d \sim 10^{-17} (\Omega \text{cm})^{-1}$ ), we find that that the pyroelectric field can remain at significant values for a few weeks. For SBN crystals, the relaxation time is much less as compared to  $\text{LiNbO}_3$ , but this increases considerably if the doping of Ce in SBN crystals  $> 0.1 \text{ wt\%}$ . So these are among the most often used crystals which are used for illustration and applications. If we consider a ferroelectric crystal, the distribution of charge present on the crystal faces cancels out the electric field induced due to spontaneous polarization and hence the net field inside a ferroelectric crystal is zero at equilibrium. A temperature change can induces a change in the spontaneous polarization resulting in an electric field  $E_{py}$ . This field is not immediately balanced and consequently, a drift current is set up analogous to the effect an external bias has on the crystal. The transient pyroelectric field  $E_{py}$  again induces a space charge field which persist to form an index waveguide supporting a soliton. The transient pyroelectric field can replace the external electric field used for screening solitons, with multiple advantages, the main being no need of identifying the  $c$ -axis since the

pyroelectric field automatically manifests along the  $c$ -axis and secondly, no need of electrodes on the crystal among others [11, 12].

### 2.4.1 Theoretical Formulation

Consider a light beam propagating along the  $z$ -axis and assume the diffraction only in  $x$ -direction. The soliton beam is polarized along the positive  $x$ -direction. The crystal is kept such that its  $c$ -axis coincides with the positive  $x$  axis. A temperature controlled (via a Peltier cell) metal plate is kept in contact with the crystal. In addition, a thermally insulating cover is kept on top of the crystal for minimizing undesirable external effects on the temperature. The incident beam can be stated as a slowly varying envelope  $\mathbf{E} = \hat{x}A(x, z) \exp(ikz)$  where  $k = k_0 n_e$ ,  $n_e$  is the unperturbed refractive index,  $n'_e$  is the refractive index along the  $c$ -axis and  $\lambda_0$  is the free space wavelength. Under these assumptions, the paraxial diffraction equation for the dynamical evolution becomes,

$$i \frac{\partial \phi}{\partial z} + \frac{1}{2k} \frac{\partial^2 \phi}{\partial x^2} - \frac{k_0 n_e^3 r_{\text{eff}} E_{\text{pysc}}}{2} \phi = 0 \quad (2.37)$$

where  $r_{\text{eff}}$  is the electro-optic coefficient,  $E_{\text{pysc}}$  is the space charge field induced solely by the pyroelectric effect [8]. It is essential to now obtain an expression for the induced space charge field  $E_{\text{pysc}}$  due to the pyroelectric effect. To this end, Ohm's law in differential form can be stated as,

$$\vec{j} = \sigma \vec{E} \quad (2.38)$$

The continuity equation is,

$$\frac{\partial \rho}{\partial t} + \nabla \cdot \vec{j} = 0 \quad (2.39)$$

While the Gauss Law states,

$$\nabla \cdot \vec{D} = \rho \quad (2.40)$$

where  $\vec{j}$  is the total current,  $\sigma = \kappa I + \sigma_d$  is the total conductivity,  $E$  is the total electric field.  $P$  is the space charge field density,  $\kappa$  is the specific photoconductivity and  $D$  is the electric displacement. The light intensity is  $I = (n_e/2\eta_0)|\phi|^2$  and is a function of  $x$  being expressed as,  $I(x) = I_0 \exp[-2(x/x_1)^2]$ .  $x_1$  is the characteristic beam radius and  $I_0$  is the maximum intensity at the beam center. Then, the total conductivity will be stated as,  $\sigma = \sigma_0 [\exp[-2(x/x_1)^2] + \eta]$  with  $\sigma_0 = \kappa I_0$  and  $\eta = I_d/I_0$  and  $I_d$  is the dark irradiance. Since we consider an SBN crystal in open circuit, and considering

the illuminated region to be narrow compared to the thickness of the crystal, total current  $j$  can be expressed as,

$$j = j_d = \sigma_d \frac{V}{H} = \sigma_d E_{py} \quad (2.41)$$

where  $j_d$  is the divergence less current which satisfies the boundary conditions. Solving (2.38)-(2.40), we get,

$$\nabla \cdot \left[ \epsilon_0 \epsilon_r \frac{\partial \vec{E}}{\partial t} + \sigma \vec{E} \right] = 0 \quad (2.42)$$

Considering the boundary conditions and assuming negligible effect of diffusion and photovoltaic effects,

$$\epsilon_0 \epsilon_r \frac{\partial \vec{E}}{\partial t} + \sigma \vec{E} = \vec{j}_d \quad (2.43)$$

Solving the partial differential Eq. (2.43),

$$E(\bar{t}, x_1) = \frac{V}{H} \left\{ \frac{\frac{\eta}{\exp(-2x^2/x_1^2) + \eta} + \frac{\eta}{\exp(-2x^2/x_1^2) - \eta}}{\exp(-2x^2/x_1^2) + \eta} \exp[-\bar{t}(\exp(-2x^2/x_1^2) + \eta)] \right\} \quad (2.44)$$

where  $\bar{t} = t/t_d$ ,  $\tau = \epsilon_0 \epsilon_r / \sigma_0$  is known as the characteristic Maxwell time. Now, two components constitute the total electric field,  $E = E_{py} + E_{pysc}$ .  $E_{py}$  is the homogeneous pyroelectric field induced by the homogeneous heating. This causes a homogeneous refractive index change.  $E_{pysc}$  is the inhomogeneous space charge field which causes an inhomogeneous refractive index change. The origin of self trapping lies in this refractive index waveguide. Hence,

$$E_{pysc} = E - E_{py} = E_{py} \frac{\exp(-2x^2/x_1^2)}{\exp(-2x^2/x_1^2) + \eta} \{ \exp[-\bar{t}(\exp(-2x^2/x_1^2) + \eta)] - 1 \} \quad (2.45)$$

For  $\bar{t} = 0$ , it is plain that  $E_{pysc} = 0$  which implies that pyroelectric field has not been screened yet in the illuminated region. At steady state, we know  $\bar{t} \gg 1$  and hence the terms in the curly brackets in (2.45) tends to  $-1$ ,

$$E_{pysc} = -E_{py} \frac{I}{I + I_d} \quad (2.46)$$

The value of the pyroelectric space charge field is dependent upon  $E_{py}$  and hence the change in temperature  $\Delta T$ . The expression is also similar to the space charge field in open circuit photovoltaics.

Substituting (2.46) into (2.37), we have,

$$i \frac{\partial U}{\partial \xi} + \frac{1}{2} \frac{\partial^2 U}{\partial s^2} + \alpha \frac{|U|^2}{1 + |U|^2} U = 0 \quad (2.47)$$

where we have used the usual dimensionless coordinates,  $\xi = z/(kx_0^2)$ ,  $s = x/x_0$ ,  $\phi = (2\eta_0 I_d/n_e)^{1/2} U$  with  $x_0$  to be an arbitrary spatial width and the intensity scaled with the dark irradiance  $I_d$ ,  $\rho = I_\infty/I_d$ ,  $\alpha = (k_0 x_0)^2 (n_e^4 r_{eff}/2) E_{py}$ .

### 2.4.2 Bright, Dark and Grey Solitons

For the solution of the bright solitons, it is now straightforward with the above theoretical foundation. Using the bright soliton ansatz,  $U = r^{1/2} y(s) \exp(iv\xi)$  with the bright soliton boundary conditions,  $y(0) = 1$ ,  $\dot{y}(0) = 0$ ,  $y(s \rightarrow \pm\infty) = 0$ .  $y(s)$  a bounded function such that  $0 \leq y(s) \leq 1$  and  $r = I(0)/I_d$ . Substituting the bright soliton ansatz in (2.47), we get,

$$\frac{d^2 y}{ds^2} = 2vy - 2\alpha \frac{ry^3}{1 + ry^2} \quad (2.48)$$

Integrating (2.48), we can obtain the soliton field profile,

$$s = \pm \int_y^1 \left\{ \frac{2\alpha}{r} [\ln(1 + r\tilde{y}^2) - \tilde{y}^2 \ln(1 + r)] \right\}^{-1/2} d\tilde{y} \quad (2.49)$$

For the dark soliton solution, using the equivalent dark soliton ansatz  $U = \rho^{1/2} y(s) \exp(i\mu\xi)$  along with the boundary conditions, we substitute in (2.47) and integrate to obtain for the spatial profile,

$$s = \pm \int_y^1 \left\{ -2\alpha \left[ \frac{y^2 - 1}{1 + \rho} - \frac{1}{\rho} \ln \left( \frac{1 + \rho\tilde{y}^2}{1 + \rho} \right) \right] \right\}^{-1/2} d\tilde{y} \quad (2.50)$$

Similarly, for the grey soliton, we shall substitute,  $U(s, \xi) = \rho^{1/2} y(s) \exp \left[ i \left( \mu\xi + \int \frac{Q ds}{y^2(s)} \right) \right]$  into (2.47) and integrate once to yield,

**Table 2.3** Typical factors of lithium niobate crystal used in our calculation [8]

Parameter	Value	Parameter	Value
$\lambda_0$	532 nm	$\epsilon_0$	$8.85 \times 10^{-12}$ F/m
$x_0$	20 $\mu$ m	$\epsilon_r$	3400
$n_e$	2.35	$\frac{\partial P}{\partial T}$	$-3 \times 10^{-4}$ Cm $^{-2}$ K $^{-1}$
$r_{\text{eff}}$	$237 \times 10^{-12}$ mV $^{-1}$	$r, \rho$	10

$$\left(\frac{dy}{ds}\right)^2 = 2\mu(y^2 - 1) - \left(\frac{1}{y^2} - 1\right)Q^2 - \frac{2\alpha}{\rho} \left[ \rho(y^2 - 1) - \ln\left(\frac{1 + \rho y^2}{1 + \rho}\right) \right] \quad (2.51)$$

The boundary conditions are,  $y^2(s = 0) = m$  ( $0 < m < 1$ ),  $\dot{y}(0) = 0$ ,  $y(s \rightarrow \pm\infty) = 1$ .

Using the boundary conditions, we can easily find,

$$Q^2 = 2\alpha \frac{\rho}{1 + \rho} - 2\mu \quad (2.52)$$

$$\mu = \frac{1}{2(m - 1)^2} \left\{ (1 - m) \left( \frac{2\alpha\rho}{1 + \rho} \right) + \frac{2m\alpha}{\rho} \left[ \rho(m - 1) - \ln\left(\frac{1 + \rho m}{1 + \rho}\right) \right] \right\} \quad (2.53)$$

The normalized intensity profile of the grey soliton can be obtained by numerically integrating (2.51) along with (2.52) and (2.53). Table 2.3 shows the typical parameters used for calculation. Using this and (2.48)–(2.52), the bright, dark and grey soliton intensity profiles have been plotted in Figs. 2.5, 2.6, 2.7 (Table 2.4).

We can see clearly in (2.49) that the quantity within brackets is positive only if  $\alpha > 0$ . So we need to take the change of temperature as positive, i.e.,  $\Delta T > 0$  and we need a heating of the crystal. Similarly, for the dark solitons, the term inside brackets in

**Fig. 2.5** Normalized spatial profile of the bright soliton for **a**  $\Delta T = 10$  °C **b**  $\Delta T = 20$  °C **c**  $\Delta T = 30$  °C (reprinted from Optik, 126, Yanli Su, Qichang Jiang, Xuanmang Ji, Photorefractive spatial solitons supported by pyroelectric effects in strontium barium niobate crystals, 1621–1624, Copyright 2015, with permission from Elsevier)

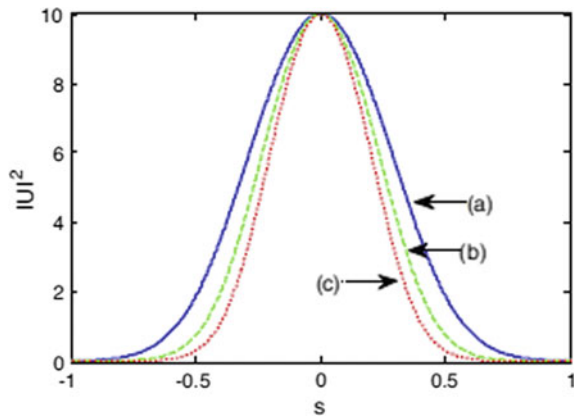


**Fig. 2.6** Normalized spatial profile of the grey soliton for **a**  $\Delta T = -10^\circ\text{C}$ ,  $m = 0.5$  **b**  $\Delta T = -10^\circ\text{C}$ ,  $m = 0.4$  **c**  $\Delta T = -10^\circ\text{C}$ ,  $m = 0.3$  (reprinted from Optik, 126, Yanli Su, Qichang Jiang, Xuanmang Ji, Photorefractive spatial solitons supported by pyroelectric effects in strontium barium niobate crystals, 1621–1624, Copyright 2015, with permission from Elsevier)

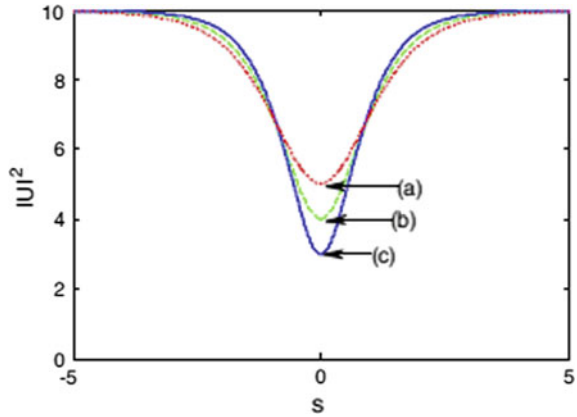


**Fig. 2.7** Normalized spatial profile of the dark soliton for **a**  $\Delta T = -10^\circ\text{C}$  **b**  $\Delta T = -20^\circ\text{C}$  **c**  $\Delta T = -30^\circ\text{C}$ . (reprinted from Optik, 126, Yanli Su, Qichang Jiang, Xuanmang Ji, Photorefractive spatial solitons supported by pyroelectric effects in strontium barium niobate crystals, 1621–1624, Copyright 2015, with permission from Elsevier)

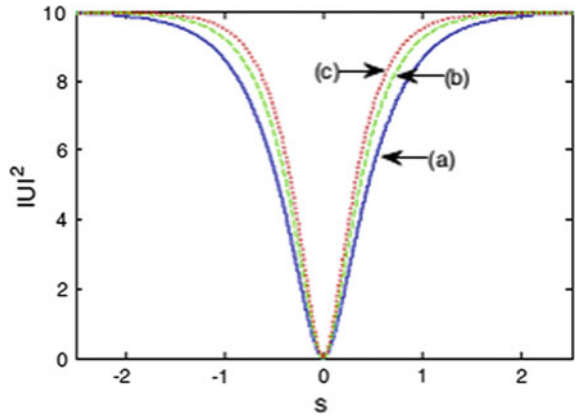


**Table 2.4** Values of  $\alpha$  for diverse values of the temperature change using Table 2.3

$\Delta T$ ( $^\circ\text{C}$ )	$\alpha$
10	20.1
20	30.2
30	40.2
-10	-20.1
-20	-30.2
-30	-40.2

(2.50) is positive only if  $\alpha < 0$ . Hence, we need a cooling of the crystal with  $\Delta T < 0$  for observing dark solitons. The same concept carries forward for grey solitons also where again we need a cooling of the crystal for their observation. The important thing to note here is that the nonlinearity is controlled by the term  $\alpha$  which is in turn dependent upon the temperature change, pyroelectric coefficient and electro-optic



coefficient. Varying these values for different types of crystals can result in different characteristics and spatial profiles of the pyroelectric solitons. (Fig. 2.6)

## 2.5 Photovoltaic Effect and Pyroelectric Solitons

Photorefractive solitons observed in steady state can be said to be broadly of three types, i.e., screening solitons, photovoltaic solitons and screening–photovoltaic solitons [3, 4, 7].

An external electric field leads to a screening of the induced space charge field and hence the name “screening solitons”. The photorefractive effect is basically a refractive index change by the electro-optic effect. The electro-optic effect comes into play because of the induced space charge field due to the drift and diffusion of photogenerated charge carriers. In case of photovoltaic solitons, the space charge field is modulated by the bulk photovoltaic field while screening photovoltaic solitons form in photorefractive photovoltaic crystals due to the combination of both the external field and bulk photovoltaic field. As we have mentioned before, replacing the external electric field with the pyroelectric field has many advantages. It is logical to now think of the combination of the external bias field, photovoltaic field and pyroelectric field and how they can have an interplay while inducing a space–charge field and in turn self trapping a light beam. Such type of solitons are screening photovoltaic pyroelectric solitons. Also, the transient pyroelectric field can be induced by externally controlled temperature changes or by absorption of the incident beam’s energy. The former case has already been seen in the previous section. In the following, we now discuss the effect of pyroelectricity due to the absorption of energy of the beam itself.

### 2.5.1 Theoretical Model

We consider the usual setup for the soliton beam as defined before. In addition, the crystal is covered with a thermally insulating cover so as to stabilize the temperature and avoid any temperature gradient. The slowly varying envelope for the incident beam reads as,  $E = \hat{x} A(x, z) \exp(ikz)$  where  $k = k_0 n_e$ ,  $n_e$  is the unchanged refractive index,  $n'_e$  is the perturbed refractive index along the direction of the extraordinary or  $c$ -axis and  $\lambda_0$  is the wavelength in free space. Beginning with the usual paraxial diffraction equation,

$$\left( i \frac{\partial}{\partial z} + \frac{1}{2k} \frac{\partial^2}{\partial x^2} + \frac{k}{n_e} \Delta n \right) A(x, z) = 0 \quad (2.54)$$

$$\Delta n = -\frac{1}{2} n_e^3 r_{\text{eff}} E_{\text{sc}} \quad (2.55)$$

Here,  $E_{sc}$  is the space charge field resulting as a consequence of both, the photovoltaic drift and the pyroelectric field. Again there are three constituent components of the total space charge field, which are the space charge field due to the external bias, the photovoltaic contribution and the pyroelectric space charge field,

$$E_{sc} = E_1 + E_2 + E_3 \quad (2.56)$$

The space charge field ( $E_1 + E_2$ ) results in biased photorefractive crystals supporting screening photovoltaic solitons. We have already studied it in detail in the previous section,

$$E_1 + E_2 = E_0 \frac{I_\infty + I_d}{I + I_d} + E_p \frac{I_\infty - I}{I + I_d} \quad (2.57)$$

The value of  $E_p$  is reliant on the state of polarization of the beam and one can infer the sign from the photovoltaic constant.  $E_{pysc}$  is the space-charge field forming as a consequence of the transient pyroelectric field  $E_{py}$  which results in turn from a change in temperature. A pulse of light can transfer energy to the material and hence induce the pyroelectric effect comparable to that brought about by a change in temperature [8, 10, 13–16]. For a short pulse of light, the pyroelectric space charge field  $E_{pysc}$  can be expressed as, [8, 10, 13–16],

$$E_3 = E_{pysc} = -\frac{1}{\varepsilon_r \varepsilon_0} \frac{\partial P_s}{\partial T} \frac{t_p}{2} \frac{\sigma_{ph}}{\varepsilon_0 \varepsilon_r} \Delta T(t) = -E_{py} \frac{t_p}{2} \frac{\sigma_{ph}}{\varepsilon_0 \varepsilon_r} \quad (2.58)$$

Now, the value of  $E_{pysc}$  is implicitly a function of the intensity of the beam. For our calculation, we need an explicit dependence and hence we approximate the space charge field as [8, 10],

$$E_{pysc} = -E_{py} \frac{t_p}{2} \frac{\sigma_{ph}}{\varepsilon_0 \varepsilon_r} \approx -E_{py} \frac{\vartheta I}{I_d} \quad (2.59)$$

where,  $t_p$  is the pulse duration,  $\sigma_{ph}$  is the photoconductivity,  $\vartheta$  is a material parameter dependent on the crystal. Since the photoconductivity  $\sigma_{ph}$  is proportional to the intensity  $I$ , this approximation is reasonable. From the values of the parameters  $E_{py}$ ,  $t_p, \varepsilon_0, \varepsilon_r$  [8, 10, 13–16], we can say that  $\frac{\lambda I}{I_d} < 1$ . Again, this can be verified independently as the pyroelectric space charge field can reach a substantial fraction of the pyroelectric field a under continuous wave laser beam [15]. The following potential condition in steady state can be used to find the value of  $E_0$ ,

$$-\int_{-l/2}^{l/2} E_{sc} dx = \varepsilon \quad (2.60)$$

where the transverse thickness of the crystal is represented by  $l$ , and the external bias is denoted by  $\varepsilon$ . Substituting (2.57)–(2.60) in (2.56), we get,

$$E_{\text{sc}} = -(\varepsilon\eta + E_p\sigma\eta - E_{\text{py}}\gamma\lambda\eta)\frac{I_\infty + I_d}{I + I_d} + E_p\frac{I_\infty - I}{I + I_d} - E_{\text{py}}\frac{\lambda I}{I_d} \quad (2.61)$$

where  $\eta = \frac{1}{\int_{-l/2}^{l/2} \frac{I_\infty + I_d}{I + I_d} dx}$ ,  $\sigma = \int_{-l/2}^{l/2} \frac{I_\infty - I}{I + I_d} dx$  and  $\gamma = \int_{-l/2}^{l/2} \frac{I}{I_d} dx$ .

Using (2.61) in the paraxial diffraction equation, we obtain the dynamical evolution equation as follows,

$$iU_\xi + \frac{1}{2}U_{\text{ss}} + \beta(|U|^2)U - \frac{\alpha(\rho - (|U|^2))}{(1 + |U|^2)}U - \delta\frac{(1 + \rho)}{(1 + |U|^2)}U = 0 \quad (2.62)$$

where we have used the previously defined dimensionless coordinates and,  $\beta = E_{\text{py}}$ ,  $\tau = (k_0x_0)^2n_e^4r_{\text{eff}}/2$ ,  $\alpha = \tau E_p$ ,  $\delta = -(\varepsilon\eta + E_p\sigma\eta - E_{\text{py}}\gamma\lambda\eta)\tau$ .

Other symbols have their meaning as defined before.

## 2.5.2 Spatial Soliton States

Using the bright soliton ansatz,  $U = r^{\frac{1}{2}}f(s)\exp(i\mu\xi)$  and substituting in (2.62),

$$\ddot{f} = 2\mu f - 2\beta(rf^2)f - 2\alpha\frac{(rf^2)f}{1 + rf^2} + 2\delta\frac{f}{1 + rf^2} \quad (2.63)$$

where  $\ddot{f} = \frac{d^2f}{ds^2}$ .

Integrating (2.63), and by use of the boundary conditions for bright solitons,

$$f^2 = 2\mu f^2 - \beta r f^4 + \frac{(2(\delta + \alpha)\log(1 + rf^2) - 2\alpha r f^2)}{r} + c \quad (2.64)$$

with

$$c = 0 \quad (2.65)$$

$$\mu = \frac{\beta r}{2} - \left(\frac{\delta}{r} + \frac{\alpha}{r}\right)\log(1 + r) + \alpha \quad (2.66)$$

Integrating (2.14) once again, we get the envelope,

$$s = \pm \int_f^1 \frac{rd\tilde{f}}{2\mu r\tilde{f}^2 - \beta r^2\tilde{f}^4 + 2(\delta + \alpha)\log(1 + r\tilde{f}^2) - 2\alpha r\tilde{f}^2} \quad (67a)$$

As  $\tilde{f}$  has to be real and bounded like  $0 \leq f(s) \leq 1$ , the sufficient condition to keep RHS positive can be inferred from (2.64),

$$-\frac{\beta r}{2} + \mu - \alpha \geq -\frac{\delta + \alpha}{r} \log(1 + r) \quad (67b)$$

For bright spatial solitons, we need positive refractive index perturbation. If we consider a lithium niobate crystal for illustration, the refractive index perturbation is negative due to there being a self-defocussing due to its negative photovoltaic coefficient. In open circuit crystals, a bright soliton can still be self trapped in the event that the self focusing induced due to the pyroelectric effect more than offsets the self-defocussing due to the photovoltaic effect [9].

If an external bias is applied, this condition is liable to be modified slightly. An external electric field applied along the  $c$ -axis results in self focussing while leading to self defocussing if applied in the opposite direction [4]. Hence, the photovoltaic self defocussing can be boosted or reduced by controlling the direction of the voltage bias. This, in turn has the tendency to change the degree of self focusing induced by the pyroelectric effect. In summary, these changes to the nonlinearity will result in an alteration of the FWHM of the soliton.

Now, with regards to the wavelength of incident light, we need to consider a wavelength for which absorption of energy is relatively large so that the heating of the crystal can take place [10]. The light absorption in LiNbO<sub>3</sub> is significant for the blue-violet light  $\sim 405$  nm [11] and hence will be used in our simulation. Now, the photoconductivity increases substantially when considering light in the blue violet region as compared to the red light and hence the photovoltaic field also decreases substantially as it is inversely proportional to the photoconductivity [17–19]. Also, the photovoltaic field has a sub-linear dependence on the incident light intensity in case of undoped LiNbO<sub>3</sub>[20]. At the chosen wavelength and intensity we consider, we should use a lesser value of  $E_p$  than that considered before for LiNbO<sub>3</sub> (in Sect. 2.4, as in [3, 6, 7]). So, a judicious conjecture would be  $E_p = -2 \times 10^5$  V/m [10]. The transient pyroelectric field is approximately taken to be  $\sim 40$  kV/cm, which correlates to a temperature change of the order of around  $\sim 10$  K in the crystal [12]. To summarize [10],  $\lambda_0 = 405$  nm,  $x_0 = 20$   $\mu$ m.,  $E_p = -2 \times 10^5$  V/m  $\sim -2$  kV/cm,  $E_{py} = 4.0 \times 10^6$  V/m,  $r_{\text{eff}} = r_{33} \sim 35 \times 10^{-12}$  m V<sup>-1</sup>,  $n_e = 2.2$ ,  $\lambda = 0.5$ ,  $r = 10$ .

With the above parameters, we obtain the value of  $\alpha = -6.846$  and  $\beta = 67.275$ . The soliton profiles for an applied voltage  $\varepsilon = \pm 4000$  V are shown in Fig. 2.8. The thickness of the crystal  $l = 10$  mm. Again, if we consider (hypothetically) the photovoltaic field constant  $E_p = +2$  kV/cm and rest of the parameters same as before, we find that the photovoltaic effect will work to support the pyroelectric effect augmenting the self trapping. This case is shown in Fig. 2.9. Hence, the interaction

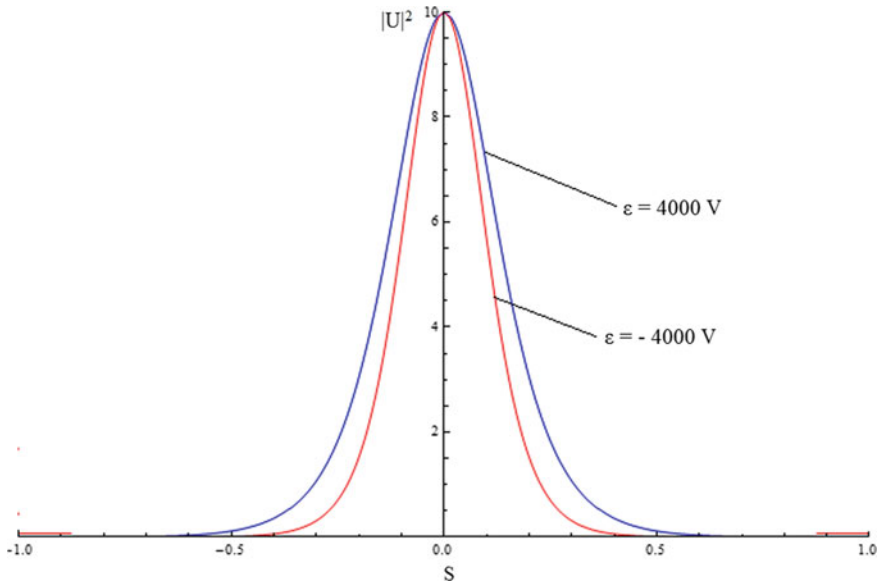


**Fig. 2.8** Spatial intensity profile of the solitons when  $\alpha = -6.846$ ,  $\beta = 67.275$ ,  $r = 10$  (reprinted from Physics Letters A, 381, Aavishkar Katti, R.A. Yadav, Spatial solitons in biased photovoltaic photo refractive materials with the pyroelectric effect, 166–170, Copyright 2017, with permission from Elsevier)

between the photovoltaic effect, external bias and the pyroelectric field can be clearly seen [10].

For the dark soliton, we take the field profile, as usual,  $U = \rho^{\frac{1}{2}}g(s)\exp(i\nu\xi)$  where  $g(s)$  is a bounded function and along with the boundary conditions of dark solitons as specified before. Substituting the dark soliton ansatz in in (2.62), we get,

$$\ddot{g} = 2\nu g - 2\beta(\rho g^2)g + 2\alpha \frac{(\rho - \rho g^2)g}{1 + \rho g^2} + 2\delta \frac{(\rho + 1)g}{1 + \rho g^2} \quad (2.68)$$

where  $\ddot{g} = \frac{d^2g}{ds^2}$ .

By using the boundary conditions at infinity in (2.68),

$$\nu = \beta\rho - \delta \quad (2.70)$$

Integrating (2.68) once,

$$\dot{g}^2 = 2\nu g^2 - \beta\rho g^4 + \frac{2\delta(1 + \rho)\log(1 + \rho g^2)}{\rho} - 2\alpha g^2$$

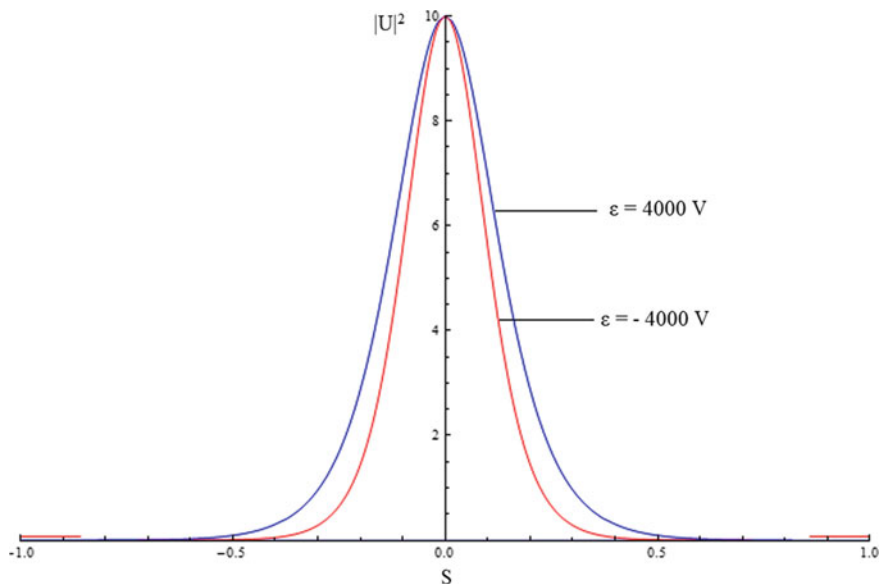


**Fig. 2.9** Spatial intensity profile of the solitons when  $\alpha = 6.846$ ,  $\beta = 67.275$ ,  $r = 10$  (reprinted from *Physics Letters A*, 381, Aavishkar Katti, R.A. Yadav, Spatial solitons in biased photovoltaic photo refractive materials with the pyroelectric effect, 166–170, Copyright 2017, with permission from Elsevier)

$$+ \frac{2\alpha(1 + \rho) \log(1 + \rho g^2)}{\rho} + 2c \quad (2.71)$$

Using the boundary conditions in (2.71) at infinity, we can obtain  $c$ ,

$$c = -v + \frac{\beta\rho}{2} + \alpha - \frac{(\alpha + \delta)(1 + \rho) \log(1 + \rho)}{\rho} \quad (2.72)$$

Integrating (2.71) using the value of  $c$  by (2.72), the soliton envelope can be derived as,

$$s = \pm \int_0^g \frac{\rho d\tilde{g}}{2v\rho\tilde{g}^2 - \beta\rho^2\tilde{g}^4 + 2(\delta + \alpha)(1 + \rho) \log(1 + \rho\tilde{g}^2) - 2\alpha\rho\tilde{g}^2 + 2\rho c} \quad (2.73)$$

Analogous to the case of bright solitons, the refractive index change is expected to be negative for self-defocussing to happen and dark solitons to form. The photovoltaic induced self defocussing should counteract the self-focussing induced by the the external bias field and the pyroelectric effect for a dark soliton to form. So, it is apt to consider the external bias values as  $\varepsilon = 4000$  V and  $\varepsilon = 40,000$  V. If the voltage bias is

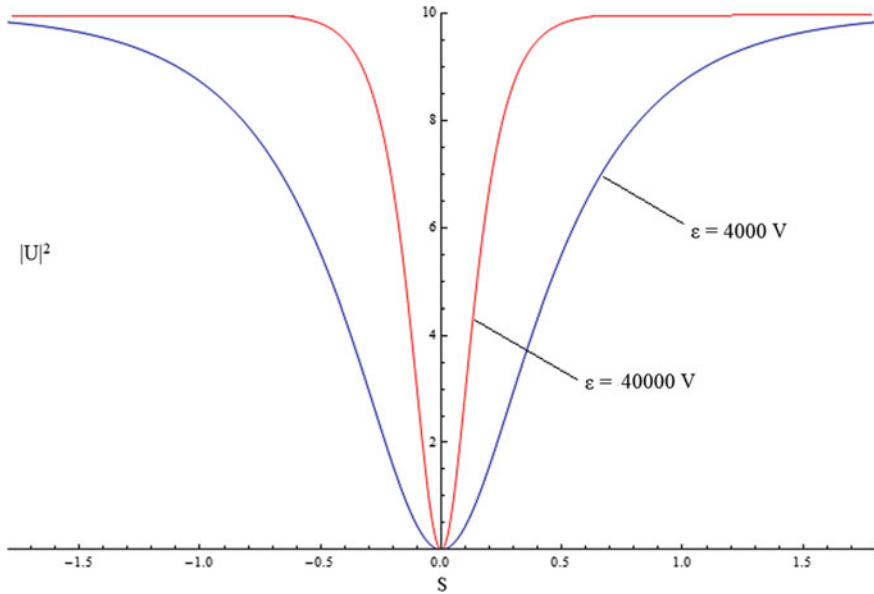


**Fig. 2.10** The normalized intensities of the solitons when  $\alpha = -6.846$ ,  $\beta = 6.7275$ ,  $\rho = 10$  (reprinted from Physics Letters A, 381, Aavishkar Katti, R.A. Yadav, Spatial solitons in biased photovoltaic photorefractive materials with the pyroelectric effect, 166–170, Copyright 2017, with permission from Elsevier)

negative, the electric field is parallel to the  $c$ -axis. So the overwhelming self focusing effect due to the induced pyroelectric space charge field prevents self defocussing. Hence, we consider [10], the following parameters,  $\lambda_0 = 405$  nm,  $x_0 = 20$   $\mu\text{m}$ .,  $E_p = -2.0 \times 10^5$  V/m,  $E_{py} = 4.0 \times 10^5$  V/m,  $r_{\text{eff}} = 35 \times 10^{-12}$  m V $^{-1}$ ,  $n_e = 2.2$ ,  $\lambda = 0.5$ ,  $\rho = 10$ . Also, we have,  $\alpha = -6.846$ ,  $\beta = 6.7275$ . The soliton profiles are shown in Fig. 2.10.

## 2.6 Concluding Remarks and Further Reading

We have studied a comprehensive theory for optical spatial solitons in photovoltaic and pyroelectric photorefractive crystals. The band transport model is used to obtain the space charge field due to photovoltaic effects and the dynamical evolution equation for light beams propagating in biased photovoltaic photorefractive crystals. The general formulation presented here branches out to systems of photorefractive crystal which is open circuited or closed circuited and without the external bias field. The pyroelectric space charge field and the dynamical evolution equation is also obtained using simple considerations of charge transport and continuity equations. Screening

photovoltaic pyroelectric solitons are studied to investigate the interplay between the pyroelectric field, external bias and photovoltaic field.

Buse [13–16] give an understanding of the different characteristics of the pyroelectric effect in photorefractive crystals. Since we focus on the theory behind the self trapping due to different configurations of pyroelectric photorefractive crystals, the author is referred to [8, 9, 11, 21] for further details of pyroliton in the experimental context. [10] has detailed exposition of screening photovoltaic pyroelectric solitons.

## References

1. P. Gunter, J.-P. Huignard (eds.), *Photorefractive Materials and Their Applications 1* (Springer Science+Business Media Inc., New York, 2006)
2. D.D. Nolte, *Photorefractive Effects and Materials*, vol. 27 (1995)
3. J.S. Liu, K.Q. Lu, Screening-photovoltaic spatial solitons in biased photovoltaic-photorefractive crystals and their self-deflection. *J. Opt. Soc. Am. B-Opt. Phys.* **16**(4), 550–555 (1999)
4. D.N. Christodoulides, M.I. Carvalho, Bright, dark, and gray spatial soliton states in photorefractive media. *J. Opt. Soc. Am. B* **12**(9), 1628 (1995). <https://doi.org/10.1364/JOSAB.12.001628>
5. N.V. Kukhtarev, V.B. Markov, S.G. Odulov, M.S. Soskin, V.L. Vinetskii, Holographic storage in electrooptic crystals: I. Steady state. *Ferroelectrics* **22**(1), 949–960 (1978). <https://doi.org/10.1080/00150197908239450>
6. G.C. Valley, M. Segev, B. Crosignani, A. Yariv, M.M. Fejer, M.C. Bashaw, Dark and bright photovoltaic spatial solitons. *Phys. Rev. A* **50**(6), R4457 (1994). <https://doi.org/10.1103/PhysRevA.50.R4457>
7. M. Segev, G.C. Valley, M.C. Bashaw, M. Taya, M.M. Fejer, Photovoltaic spatial solitons. *J. Opt. Soc. Am. B* **14**(7), 1772 (1997). <https://doi.org/10.1364/JOSAB.14.001772>
8. Y. Su, Q. Jiang, X. Ji, Photorefractive spatial solitons supported by pyroelectric effects in strontium barium niobate crystals. *Optik* **126**(18), 1621–1624 (2015). <https://doi.org/10.1016/j.ijleo.2015.04.053>
9. J. Safioui, F. Devaux, M. Chauvet, Pyroliton: pyroelectric spatial soliton. *Opt. Express* **17**(24), 22209–22216 (2009). <https://doi.org/10.1364/OE.17.022209>
10. A. Katti, R.A. Yadav, Spatial solitons in biased photovoltaic photorefractive materials with the pyroelectric effect. *Phys. Lett. Sect. A: Gen. At. Solid State Phys.* **381**(3), 166–170 (2017). <https://doi.org/10.1016/j.physleta.2016.10.054>
11. S.T. Popescu, A. Petris, V.I. Vlad, Fast writing of soliton waveguides in lithium niobate using low-intensity blue light. *Appl. Phys. B: Lasers Opt.* **108**(4), 799–805 (2012). <https://doi.org/10.1007/s00340-012-5202-7>
12. S.T. Popescu, A. Petris, V.I. Vlad, Recording of self-induced waveguides in lithium niobate at 405 nm wavelength by photorefractive–pyroelectric effect. *J. Appl. Phys.* **113**(21), 213110 (2013). <https://doi.org/10.1063/1.4808321>
13. K. Buse, Light-induced charge transport processes in photorefractive crystals I: models and experimental methods. *Appl. Phys. B: Lasers Opt.* **64**(3), 273–291 (1997). <https://doi.org/10.1007/s003400050175>
14. K. Buse, K.H. Ringhofer, Pyroelectric drive for light-induced charge transport in the photorefractive process. *Appl. Phys. A Solids Surf.* **57**(2), 161–165 (1993). <https://doi.org/10.1007/BF00331438>
15. K. Buse, R. Pankrath, E. Krätzig, Pyroelectrically induced photorefractive effect in Sr(0.61)Ba(0.39)Nb(2)O(6):Ce. *Opt. Lett.* **19**(4), 260–262 (1994). <https://doi.org/10.1364/OL.19.000260>



16. N. Korneev, D. Mayorga, S. Stepanov, A. Gerwens, K. Buse, E. Krätzig, Enhancement of the photorefractive effect by homogeneous pyroelectric fields. *Appl. Phys. B* **66**, 393 (1998)
17. J.R. Schwesyg, M.C.C. Kajiyama, M. Falk, D.H. Jundt, K. Buse, M.M. Fejer, Light absorption in undoped congruent and magnesium-doped lithium niobate crystals in the visible wavelength range. *Appl. Phys. B: Lasers Opt.* **100**(1), 109–115 (2010). <https://doi.org/10.1007/s00340-010-4063-1>
18. M. Alonzo et al., Self-confined beams in erbium-doped lithium niobate. *J. Opt. A: Pure Appl. Opt.* **12**(1), 015206 (2010). <https://doi.org/10.1088/2040-8978/12/1/015206>
19. F. Lüdtke, N. Waasem, K. Buse, B. Sturman, Light-induced charge-transport in undoped LiNbO<sub>3</sub> crystals. *Appl. Phys. B: Lasers Opt.* **105**(1), 33–50 (2011). <https://doi.org/10.1007/s00340-011-4615-z>
20. R. Jungen, G. Angelow, F. Laeri, and C. Grabmaier, Efficient ultraviolet photorefractive in LiNbO<sub>3</sub>. *Appl. Phys. A Solids Surf.* **55**(1), 101–103 (1992). <https://doi.org/10.1007/BF00324609>
21. S.T. Popescu, A. Petris, V.I. Vlad, Recording of self-induced waveguides in lithium niobate at 405 nm wavelength by photorefractive-pyroelectric effect. *J. Appl. Phys.* **113**(21), 2013. <https://doi.org/10.1063/1.4808321>